Contents lists available at ScienceDirect

Journal of Power Sources

journal homepage: www.elsevier.com/locate/jpowsour



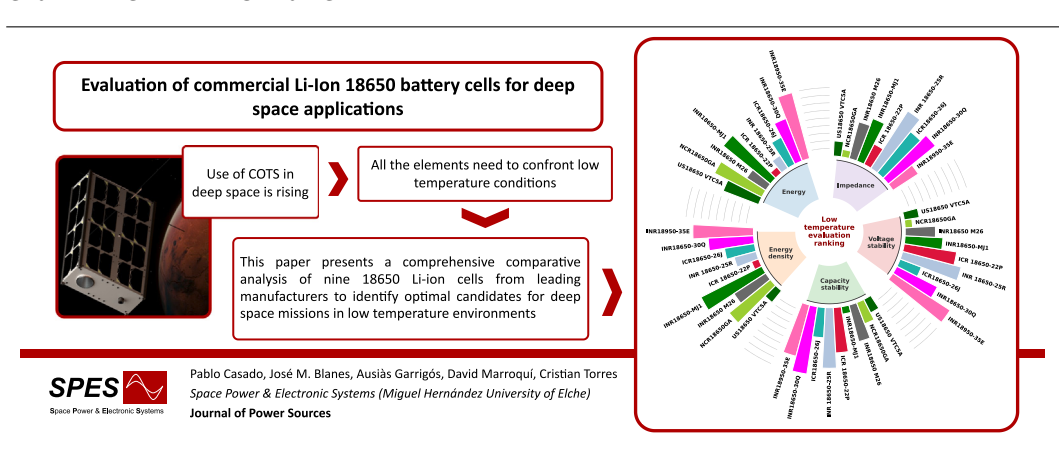


Evaluation of commercial Li-Ion 18650 battery cells for deep space applications

P. Casado[®]*, J.M. Blanes[®], A. Garrigós, D. Marroquí[®], C. Torres

Space Power & Electronic Systems (Miguel Hernández University of Elche), Avinguda de la Universitat d'Elx, S/N, Elche, 03202, Spain

GRAPHICAL ABSTRACT



HIGHLIGHTS

- ullet Performance evaluation of nine 18650 cells under low-temperature conditions.
- · Effects of low temperatures on the internal impedance of selected cells.
- · Selection of the most suitable cell model for space missions in cold conditions.
- Promote the use of commercial 18650 cells in CubeSats on deep space missions.

ARTICLE INFO

Keywords: 18650 Lithium-Ion Battery Electrochemical Impedance Spectroscopy Commercial Off-The-Shelf (COTS) CubeSat Deep-Space

ABSTRACT

The adoption of Commercial Off-The-Shelf components in the space sector has significantly grown in recent years, with 18650 Li-Ion battery cells emerging as a reliable solution for energy storage in small satellites. This paper presents a comprehensive comparative analysis of nine 18650 Li-Ion cells from leading manufacturers to identify an optimal candidate for deep space missions in low temperature environments. Critical performance parameters such as energy capacity, energy density, low-temperature capacity retention, voltage stability, and thermal behavior were assessed through discharge tests and Electrochemical Impedance Spectroscopy measurements. The findings underscore the importance of selecting cells based on temperature-dependent performance characteristics rather than solely relying on nominal specifications. This study provides valuable insights into the design of efficient and reliable energy storage systems for deep space microsatellite missions.

E-mail addresses: pcasado@umh.es (P. Casado), jmblanes@umh.es (J.M. Blanes), augarsir@umh.es (A. Garrigós), dmarroqui@umh.es (D. Marroquí), c.torres@umh.es (C. Torres).

https://doi.org/10.1016/j.jpowsour.2025.236552

Received 26 November 2024; Received in revised form 20 January 2025; Accepted 13 February 2025 Available online 27 February 2025

^{*} Corresponding author.

1. Introduction

With the advent of the CubeSat standard, the space industry has undergone significant transformation in recent years. These small, standardized satellites offer a cost-effective and agile platform for a variety of space missions [1,2]. Additionally, the flexibility and affordability of CubeSats have led to their widespread adoption for Low Earth Orbit (LEO) missions. However, extending CubeSat missions into deep space presents new challenges and opportunities. According to [3], deep space missions involve navigating and operating in environments far from Earth's protective atmosphere and magnetic field, introducing additional considerations for thermal management, power generation, communication, propulsion and radiation hardness.

One of the primary challenges for space missions, both deep space and terrestrial orbiters, is managing extreme temperatures [4]. While both mission types face harsh thermal conditions, deep space missions encounter additional difficulties due to reduced solar radiation, which affects the power available for thermal management systems. Low temperatures can significantly impact the performance and lifespan of onboard systems, especially batteries and electronic components. Fig. 1 illustrates the superficial temperature of a microsatellite according to its external color, during illumination and eclipse periods, and as a function of its distance from the Sun. Additionally, the figure highlights several interesting destinations for a CubeSat mission, including planets such as Mercury, Venus and Mars, along with alternative destinations like the near-Earth asteroid Apophis and the dwarf planet Ceres. These temperature fluctuations can slow down electrochemical reactions within batteries, leading to reduced capacity and increased internal resistance, as described in [5]. Consequently, this diminishes power output and can potentially result in mission failure due to improper battery management [6].

To address these challenges, robust thermal management strategies are essential. These may include the use of advanced insulation materials, active heating elements, and innovative thermal regulation techniques to maintain operational temperatures. Furthermore, selecting components with proven performance under extreme conditions is critical for mission success.

In the late 1990s, commercial off-the-shelf (COTS) lithium-ion (Liion) cells began gaining popularity across various industries. This trend extended to the space industry, which started considering these battery cells for small satellites [7]. Early in the 21st century, the first space applications using Li-ion cells were launched (e.g., PROBA-1, Mars Express [8]). The success of these missions marked the beginning of COTS Li-Ion battery adoption in space applications [9].

Several studies comparing commercial 18650 Li-Ion battery cells can be found in the literature, see for example [10–14]. These studies primarily focus on such as capacity fade after repeated charge-discharge cycles and impedance measurements at different states of charge. For aerospace applications, NASA researchers conducted a detailed evaluation of commercial 18650 cells in [15], analyzing cycle life under varying temperatures and characterizing them using Electrochemical Impedance Spectroscopy (EIS). However, none of these studies thoroughly analyzed cell behavior at low temperatures.

Although the optimal operating range for this type of battery is well-established, it is essential to analyze performance beyond safe operating conditions. This paper introduces a novel discussion of the performance of nine different commercial 18650 Li-Ion cells for potential use in a CubeSat operating at low temperatures. By evaluating these cells, the study identifies the most suitable options to ensure reliable power supply and mission success in the harsh conditions of deep space.

The key contributions of this article are outlined below:

- Performance evaluation under extreme conditions: This article provides an in-depth assessment of the behavior of 18650 cells under low-temperature conditions and varying discharge rates.
- Impact of temperature on impedance and energy efficiency: Using Electrochemical Impedance Spectroscopy (EIS), this article analyzes the effects of low temperatures on the internal impedance of the cells.

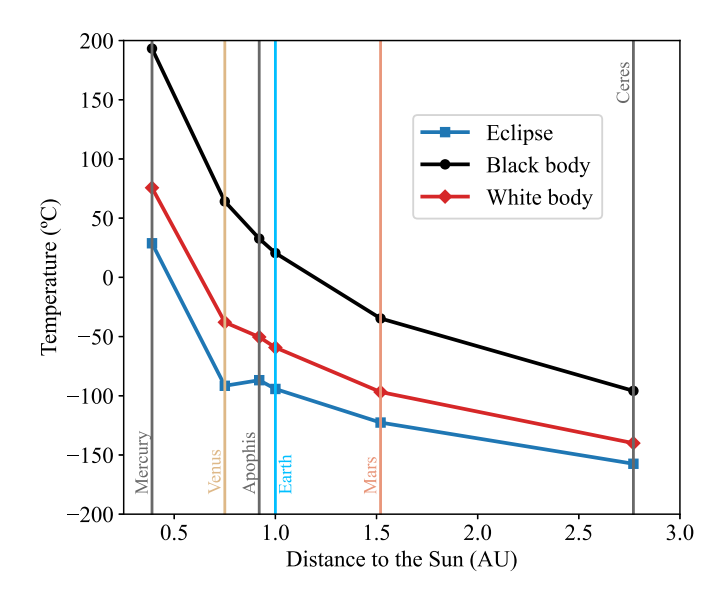


Fig. 1. Superficial temperature for a CubeSat in some interest points.

- 3. Cell comparison for optimal selection: By comparing nine cells from different manufacturers with diverse specifications, this research identifies the models that offer superior performance in terms of discharge capacity, energy efficiency, and stability at low temperatures. This information supports the selection of the most suitable cells for space missions inside of the cold and hostile environment of deep space.
- 4. Advancement of knowledge in cost-effective energy solutions for space exploration: With the low cost and widespread availability of 18650 cells, the results of this study could promote their use in cost-effective space exploration missions, such as CubeSats and microsatellites. The findings provide evidence of their viability for challenging space environments.

2. Experimental

2.1. Cells under test

As previously discussed, Commercial Off-The-Shelf (COTS) Li-ion 18650 cylindrical cells have been identified as a practical solution for CubeSat energy storage systems. This study compares nine different commercial 18650 Li-ion cell models from Samsung-SDI, LG-Chem, Panasonic, and Sony. These manufacturers were selected based on their identification as high-quality suppliers by NASA [15]. The selected cell models include 35E, 30Q, and 25R from Samsung, MJ1 from LG, and GA from Panasonic due to their applicability in space missions [15–17]. Additionally, the Sony VTC5A model was included for its low variability in mass production [18]. To provide a broader comparison, three other popular commercial 18650 models (26J and 22P from Samsung, and M26 from LG) were also evaluated.

For statistical purposes and to eliminate potential anomalies, five cells from each model and batch were used in each test. All cells were unused and brand-new when characterized. To prevent storage fading [19,20], the cells were stored at 20 $^{\circ}$ C in a dry environment and maintained at a voltage of 3.7 V.

Minimal variation was observed among cells of the same model. Hence, the results presented correspond to a random sample from each group of five.

Table 1 summarizes the key parameters of the cells used in this study. The mass data has been verified by calculating the average across five samples per cell model, with a measurement error margin of ± 0.1 g.

Table 1 18650 battery cells characteristics.

Manufacturer	Model number	Batch number	Capacity (mAh)	Max. Current (A)	Nominal voltage (V)	Min. Voltage (V)	Mass (g)	Energy density (Wh/kg)
Samsung SDI	INR18650-35E	MJ1T	3500	8	3.6	2.65	48.2	261.4
Samsung SDI	INR18650-30Q	NH3T	2950	15	3.6	2.5	45.8	231.9
Samsung SDI	ICR18650-26J	TLZ1	2600	5.2	3.63	2.75	44.0	214.5
Samsung SDI	INR18650-25R	MG4T	2500	20	3.6	2.5	42.8	210.3
Samsung SDI	ICR18650-22P	5LQ4	2200	10	3.62	2.75	43.2	184.4
LG CHEM	INR18650-MJ1	GB182G013N1	3500	10	3.635	2.5	46.8	271.8
LG CHEM	INR18650-M26	GA050B193A1	2600	10	3.65	2.75	42.6	222.8
Panasonic/Sanyo	NCR18650GA	MH12210	3300	10	3.6	2.5	46.4	256.0
SONY	US18650 VTC5A	K 5AA13ZI01N	2600	35	3.6	2.5	45.25	206.9

2.2. Equipment

To ensure precise control of testing conditions and high-resolution data acquisition, specialized equipment was employed. Cells were charged and discharged using ITECH IT-3612 bidirectional DC power supplies. For data acquisition, a DAQ34970A from Agilent has been employed. The EIS test was performed using a HIOKI BT4560 and its associated battery impedance meter application. Complementary, the HIOKI Probe L2003 has been used.

All the tests were performed inside a climatic chamber under controlled environmental temperature. The superficial temperature of each cell was continuously monitored by measuring the impedance of Pt100 sensors positioned on the cell surfaces, allowing for accurate tracking throughout the testing process.

2.3. Test conditions

Concerning the tests that have been performed in this study, some considerations have been made to ensure a comprehensive evaluation.

On the one hand, to minimize the impact of the charging process, all cells were charged with the Constant Current Constant Voltage (CCCV) method. Initially, the current was set to 1 A, and when the voltage reached 4.2 V, the voltage was held at 4.2 V until the current dropped to 20 mA. As demonstrated in [21], using low charging currents with this protocol significantly reduces efficiency losses.

On the other hand, the temperature has been considered. During the charging period, the environmental temperature has been set to 25 °C, which is an optimal temperature for this process [22]. In fact, lower charging temperatures are known to accelerate battery aging [23]. In addition, to guarantee the temperature in the cells, a three-hour settling time has been established between temperature changes. This settling time has also allowed to standardize the testing conditions and reduce the effect of the resting time on the battery impedance [24].

There are many types of tests that can be used to evaluate battery performance. In this study, two primary characterization methods have been used: Discharge test and EIS test.

2.3.1. Discharge test

In space applications, understanding the performance of electrical components, particularly Li-ion batteries, is critical. Factors such as temperature, discharge current, and total internal resistance affect parameters like discharge capacity, open circuit voltage, and terminal voltage [25]. Therefore, discharge curves for each battery model were analyzed under conditions including temperatures of 25 °C, 0 °C, -20 °C, and -30 °C. These temperatures were chosen because lower temperatures often prevent successful discharge due to high internal impedance.

Discharge currents of 0.2 A, 0.5 A, and 1 A were used, reflecting typical load conditions for CubeSat applications. According to the literature, common battery bus configurations for microsatellites include nominal voltages of 7.2 V (2S), 14.4 V (4S), and 28.8 V (8S) [16]. At the highest discharge rate (1 A), instantaneous load power provided by the battery ranges from 5.4 W to 33.6 W, depending on the configuration and state of charge.

2.3.2. Electrochemical impedance spectroscopy test

EIS measurements were also conducted. This technique measures internal resistance and reactance in response to an AC stimulus, providing insights into electrochemical behavior, as is detailed in [26,27]. From a mechanism perspective, both DC techniques and EIS can be utilized to identify battery impedance and their related electrochemical processes, and DC impedance measurement can yield results equivalent to EIS. However, DC impedance measurement is underdeveloped at present and its implementation in real-life application is challenging, and many parameters (e.g., time constants of electrochemical processes) cannot be accurately determined [28]. Nevertheless, with the development of new computational methods and machine learning algorithms [29], it is expected that accurate battery health status and fault diagnosis [30] will be obtained directly from DC testing in the near future.

In this study, all the EIS tests were performed with a 100% State of Charge (SOC) across a frequency range from 0.01 Hz to 1 kHz. According to the manual of the battery impedance meter used (HIOKI BT4560), when working in the impedance range of 100 m Ω the test is performed with a stimulus current of 50 mA rms, this parameter is not configurable. Moreover, measurements have been done in medium speed mode, which measures two times each frequency in the range of 0.01 Hz to 66 Hz, eight times in the range of 67 Hz to 250 Hz and 32 times in the range of 260 Hz to 1050 Hz.

To examine the temperature dependency, EIS characterizations were performed under controlled environmental temperatures, specifically at 25 °C, 10 °C, 0 °C, -10 °C, -20 °C, and -30 °C.

For accurate battery characterization, equivalent circuit models are commonly employed. The selection of an appropriate circuit model depends on three characteristics: the shape of the graph, the frequency bandwidth and the physical properties of the battery materials. The proposed model in Fig. 2 is based on [31,32], providing a generic model suitable for the type of cells used in this work. This approach ensures that the chosen model effectively captures the cells' behavior across the tested temperature and frequency ranges.

In this electrical model, the inductor (L) and the resistance (R_L) are associated with the wiring effects of the cells, that affects the higher frequencies. $R_{\rm S}$ characterizes the electrolyte of the cells. Next, two Zarc elements in series model the middle frequencies. Each one is composed of the parallel connection between a constant phase element and a resistor (R_1 and $\text{CPE}_1,\,R_2$ and CPE_2). Finally, a Warburg element (W_E) in series models the low frequencies. Their purpose is to provide information about the internal changes in the battery cell.

3. Results

The following section presents a comprehensive analysis of the cells' performance under controlled conditions. The results are divided into two main subsections: Cell Discharging Performance, which examines the discharge behavior across various temperatures, and EIS Analysis, which provides insights into the cells' impedance characteristics through electrochemical impedance spectroscopy. Together, these findings illustrate the influence of temperature and discharge conditions on the electrochemical properties and overall efficiency of the cells.

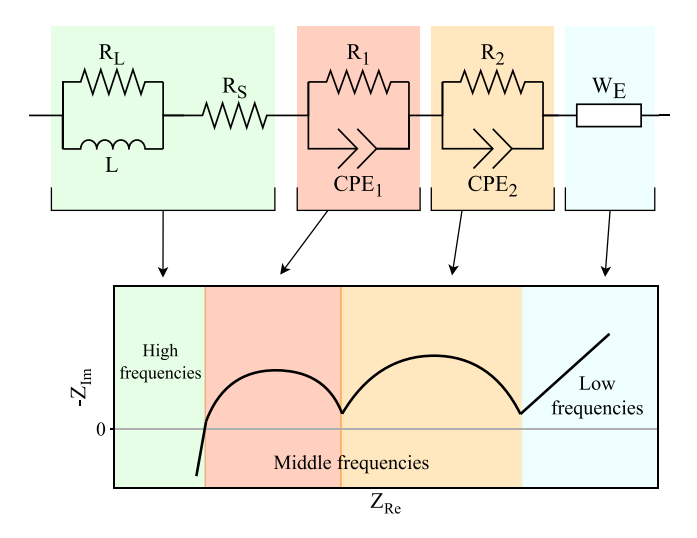


Fig. 2. EIS 18650 Battery cell equivalent circuit model.

3.1. Cell discharging performance results

This subsection provides an in-depth analysis of the discharge characteristics of each cell, focusing on how they perform under the defined testing conditions. Discharge behavior is a critical factor in assessing cell reliability, particularly for applications in extreme environments, as it directly impacts energy availability and thermal stability. Fig. 3 presents the discharge curves for all tested cells' models, illustrating variations in voltage and capacity profiles across different temperatures. These curves serve as a baseline for further analysis, enabling a detailed comparison of each cell's response to temperature and discharge rate.

It is worth noting that, at -30 °C and 1 A discharge current, cells INR18650-MJ1, NCR18650GA and US18650-VTC5A experienced immediate voltage drops below the minimum threshold, resulting in unobservable discharge curves.

To further understand the factors affecting discharge performance, three parameters are analyzed: Capacity reduction, Initial Voltage, and Temperature Rising.

3.1.1. Capacity reduction

This section examines the capacity variation as a function of temperature. Table 2 summarizes all the measured capacities at different temperatures and discharge currents, while Table 3 lists the total energy output. In order to address a visual representation of the results, Fig. 4 presents this variation in two parts. The first row shows the measured capacity for each battery model at different temperatures and discharge rates. As observed, cells with initially larger capacities experience a more pronounced decrease in capacity compared to those with lower nominal capacities. This is because high energy cells have typically thicker electrodes [33], which can enhance the energy density of the cell up to a certain limit [34]. However, higher electrode thickness increases the risk of lithium plating and gets worse behavior at lower temperatures, as is commented in [35].

To provide a clearer comparison of these capacity losses, the second row of Fig. 4 illustrates the relative capacity changes. This relative capacity was calculated using the nominal capacities included in Table I. It is important to note that the end-of-discharge voltage is set at 2.8 V for all cells under test. Since not all cells are designed to discharge to the same minimum voltage according to their manufacturer's specifications, some cells in this test may not deliver their full theoretical energy. However, the primary purpose here is to observe the trend in capacity loss as temperature decreases, rather than to measure absolute energy output for each cell.

Next the result of the capacity reduction tests for each cell are summarized:

- INR18650-35E: This cell is the one with the highest capacity in all working conditions with a capacity reduction of 30% in the worst condition.
- 2. INR18650-30Q. This cell has a high-capacity retention capability in the measured temperature range. The capacity of these cells has only decreased around 20% in the worst condition. Besides, it is the second cell with highest capacity when working at -30~°C.
- 3. ICR18650-26J. The influence of low temperatures on the capacity loss of this cell is considerable, with a reduction of around 50% of its nominal capacity at -30 °C.
- 4. INR 18650-25R. Although it is the cell with second lowest capacity at 25 $^{\circ}$ C, its behavior at low temperatures is remarkable, it has a high-capacity retention capability, and it is the third cell with highest capacity at -30 $^{\circ}$ C.
- 5. ICR 18650-22P. This is the cell with the original lowest capacity. However, as INR 18650-25R, its behavior at low temperatures is remarkable, it has a high-capacity retention capability.
- 6. INR18650-MJ1, NCR18650GA and US18650 VTC5A. The capacity of these three cells is strongly influenced by low temperatures being unusable at $-30~^{\circ}$ C.
- 7. INR18650 M26: This cell has a curious behavior, due to its high self-heating capability during the discharge process it works better at lower temperatures with higher discharge currents.

3.1.2. Initial voltage

Another important factor to consider in the discharge curves is the initial voltage of each cell at the start of the discharge. Fig. 5A shows the initial voltages for all cells across different temperatures and discharge rates. This representation is essential because the initial voltage drop indicates how effectively the battery bus will maintain the desired voltage range in microsatellite applications. If this voltage drop is higher than expected, it could fall outside the working voltage range, and it can affect the system performance.

Next the result of initial voltage tests for each cell are summarized.

- INR18650-35E and INR18650-30Q are the cells with highest initial voltage in all discharge working conditions, with an initial voltage higher than 3.4 V.
- ICR18650-26J, INR 18650-25R, ICR 18650-22P and INR18650-MJ1. All of these cells have an initial voltage in all conditions higher than 3.1 V.
- 3. NCR18650GA and US18650 VTC5A and INR18650 M26. These three cells are strongly influenced by low temperatures having an initial voltage at $-30~^{\circ}$ C 1 A lower than 3 V.

3.1.3. Cell temperature during discharge

This section examines the increase in cell surface temperature during discharge, focusing on how thermal behavior affects both the efficiency and safety of the cells under load. The heat generated during discharge is due to the Joule effect [36], where the internal resistance of each cell converts a portion of the electrical energy into thermal energy as current flows through the cell. As is discussed in [37], this phenomenon causes cells to heat up during discharge, with higher discharge currents producing greater amounts of heat. As expected, decreasing the discharge current leads to a reduced temperature increase, underscoring the direct relationship between current intensity and thermal response.

To further illustrate the thermal impact of discharge, Fig. 5B includes four graphs. Each one shows the maximum temperature reached by every cell at different ambient temperatures.

It is worth noting that the temperature rise is higher at lower ambient temperature and higher discharge current. This behavior is interesting at low temperatures because, as it can be seen in cell INR18650 M26, it works better at low temperatures with higher discharge currents due to its self-heating.

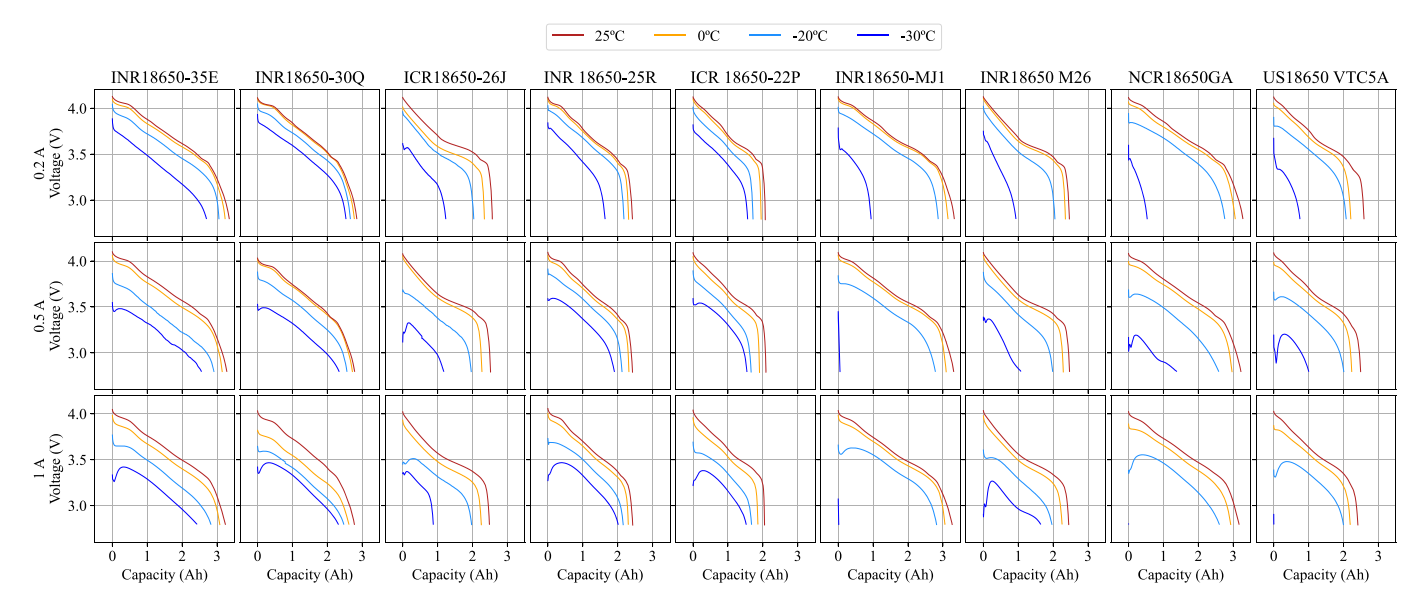


Fig. 3. Discharge curves of each battery cell at different temperatures and discharge currents. The first row corresponds to a discharge current of 200 mA, the second row to 500 mA, and the third row to 1 A. Each column corresponds to a one battery cell model. Each color corresponds to a different ambient temperature. (For interpretation of the references to color in this figure legend, the reader is referred to the web version of this article.)

Table 2
Measured capacities in mAh of all the cells at different discharge currents and temperatures.

Discharge current (A)	Temperature (°C)	INR18650-35E	INR18650-30Q	ICR18650-26J	INR 18650-25R	ICR 18650-22P	INR18650-MJ1	INR18650 M26	NCR18650GA	US18650 VTC5A
	25 0	3349.53 3229.98	2844.49 2772.76	2567.87 2400.83	2423.17 2314.13	2069.85 1952.08	3326.02 3145.51	2464.31 2350.46	3275.56 3056.48	2587.49 2330.44
0.2	-20	3229.98	2659.74	2036.41	2179.07	1718.56	2863.99	2049.16	2755.94	2076.09
	-30	2694.25	2532.80	1233.86	1638.55	1563.61	941.83	931.40	534.07	750.18
	25	3279.41	2781.29	2517.16	2425.36	2089.47	3308.43	2468.99	3219.67	2491.03
	0	3147.36	2718.17	2271.08	2322.54	1905.03	3093.93	2290.25	2965.09	2235.95
0.5	-20	2910.67	2561.29	1963.23	2124.51	1664.51	2782.63	1985.41	2580.43	2008.14
	-30	2548.68	2335.00	1175.03	1905.32	1543.99	52.03	1070.00	1373.73	1001.51
1	25	3238.00	2775.50	2485.87	2431.58	2049.70	3265.70	2446.46	3165.82	2412.02
	0	3078.80	2617.61	2253.93	2305.53	1859.48	3059.15	2255.20	2927.96	2191.85
	-20	2821.83	2470.37	1974.23	2158.29	1675.87	2818.93	1963.63	2599.95	1996.86
	-30	2418.14	2313.57	876.11	2013.62	1522.22	16.47	1637.79	0.84	4.46

3.2. EIS measurements results

In this study, measurements were conducted with a 4.2 V charge level for each cell, chosen specifically because, in microsatellite applications, batteries are often operated with shallow depth-of-discharge (DOD) [38]. This voltage setup aligns with typical operational conditions, providing relevant data for low DOD scenarios encountered in space missions.

The EIS instrument used has a measurement range limited to $100~\text{m}\Omega$, with a 50 mA RMS current for measurements within this range. At lower temperatures, the cells exhibit increased impedance, often surpassing this $100~\text{m}\Omega$ limit. Consequently, at the lowest temperatures tested, impedance values could not be measured across the entire frequency range. This limitation affects low-temperature measurements. However, the results still offer valuable insight into how temperature impacts internal resistance and overall impedance profiles under realistic microsatellite operating conditions.

Fig. 6 shows the EIS measurements of the cells, where the experimental data points are represented as circle markers, and the fitted

curves are shown as dotted lines. The fitted curves are derived from the model outlined in the experimental section (see Fig. 2), illustrating the comparison between the measured impedance and the theoretical behavior predicted by the model.

The EIS measurements, by Nyquist diagram in Fig. 6, are also analyzed by separating the real and imaginary components of the impedance in Fig. 7. This new representation provides a clearer understanding of the individual contributions to total impedance, allowing to observe the resistive behavior through the real component and the capacitive behavior through the imaginary component. As discussed in [39], higher values in the real part are traduced to a lesser efficiency, and higher values of the negative imaginary part correspond to a slower response of the cell, especially at low frequencies.

It is important to note that, due to the $100~\text{m}\Omega$ measurement range of the EIS device previously described, some measurements could not be completed across the entire frequency range, particularly at lower temperatures where the impedance values exceed this limit. Nevertheless, as can be seen in Fig. 7, the results clearly show an increase in the real component of the impedance as the temperature decreases.

Table 3
Discharged energy in Wh of all cells at different discharge currents and temperatures.

Discharge current (A)	Temperature (°C)	INR18650-35E	INR18650-30Q	ICR18650-26J	INR 18650-25R	ICR 18650-22P	INR18650-MJ1	INR18650 M26	NCR18650GA	US18650 VTC5A
0.2	25	12 285.95	10 437.66	9422.48	8955.42	7686.70	12 165.34	9013.43	11 966.31	9472.00
	0	11 806.62	10 173.44	8394.88	8539.66	7215.23	11 532.09	8554.60	11 142.30	8073.15
	-20	10 903.73	9591.72	7191.08	7902.32	6204.25	10 266.27	7253.10	9729.77	7288.02
	-30	9068.73	8826.29	4096.34	5679.24	5390.22	3172.45	3104.27	1715.76	2407.42
0.5	25	11 923.81	9991.42	9108.71	8888.57	7671.44	11 981.52	8916.30	11 651.46	9045.03
	0	11 322.29	9741.53	8170.71	8450.83	6920.16	11 203.65	8192.23	10 654.42	8053.09
	-20	9839.92	8851.92	6632.84	7506.01	5819.39	9626.89	6792.27	8661.48	6786.36
	-30	8204.16	7557.39	3684.42	6383.24	5171.88	161.92	3345.23	4124.32	3075.20
1	25	11 584.85	9923.25	8815.54	8799.11	7411.92	11 629.96	8655.18	11 275.45	8627.87
	0	10 816.66	8977.82	7829.36	8259.15	6596.12	10 851.19	7860.69	10 256.96	7712.11
	-20	9449.69	8173.42	6525.99	7405.97	5648.05	9584.65	6447.97	8613.67	6568.66
	-30	7694.58	7472.61	2832.48	6571.67	4877.84	47.67	4967.66	2.04	12.58

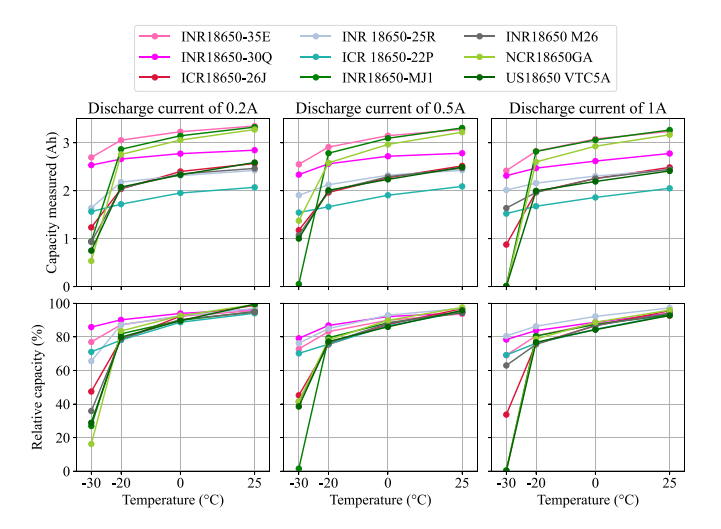


Fig. 4. The first row refers to the measured capacity of each battery model at different temperatures and the second row is associated with the relative capacity. Each column corresponds to a different discharge current. Each color corresponds to a different battery cell model. (For interpretation of the references to color in this figure legend, the reader is referred to the web version of this article.)

In order to analyze the results of Figs. 6 and 7 in depth, the parameters extracted from the equivalent circuit model have been studied. In the appendix I 'Supplementary data', all the parameters of the model and the representation of the real part and the imaginary part are presented. However, only the R_2 values are presented in this section, because this is the most significant parameter for this study. As the temperature decreases, the R_2 value becomes higher. This parameter is associated with the charge transfer resistance at the electrodes [31], which becomes increasingly relevant at low temperatures [40,41]. Table 2 shows the R_2 values for each cell across various temperatures.

As can be seen in Table 3, cells ICR18650-26J and INR 18650-25R have the lowest transfer resistances at low temperatures, lower than 100 m Ω . Cells INR18650-35E, INR18650-MJ1, INR18650 M26, NCR18650GA and INR18650-30Q have a transfer resistance lower than 525 m Ω at -30 °C. On the other hand, cells ICR 18650-22P and US18650 VTC5A have a very high transfer resistance (see Table 4).

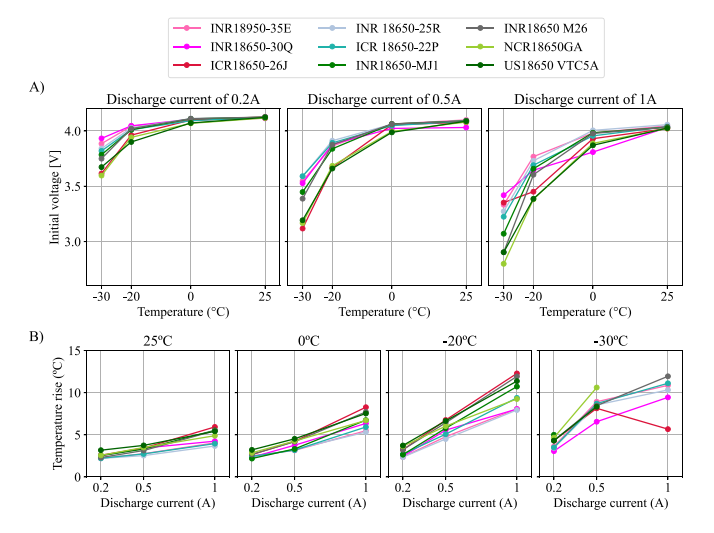


Fig. 5. (A) Initial voltages of the discharges at different temperatures. Each graph corresponds to a specific current discharge rate. (B) Maximum temperatures reached during each discharge. Each graph refers to a specific environmental temperature. Each color corresponds to a different battery cell model. (For interpretation of the references to color in this figure legend, the reader is referred to the web version of this article.)

4. Discussion

The results of this study allow a comparative assessment of the cells under test, identifying which are best suited for deep space microsatellite missions. The results of the discharge performance test, and the EIS measurements are discussed in this section. The purpose of this analysis is to provide insight into each cell's strengths and limitations.

4.1. Cell discharging performance analysis

Cell discharge tests results are an important guiding principle in a battery cell model selection process. These tests have verified the energy available in each cell model at each temperature. Analyzing the capacity measured, represented in Fig. 4, it becomes evident that the INR18650-25R and ICR18650-22P cells, despite having a lower nominal capacity, can deliver more energy at low temperatures compared to other cells with higher nominal capacities. This fact highlights the importance of considering temperature-dependent performance, rather than only the nominal capacity, when selecting cells for applications in cold environments. Among all the cells tested, the INR18650-25R and

Table 4 Charge transfer resistance at the electrodes measured values (m Ω) of each cell at different temperatures.

Cell model	Temperature								
	25 °C	10 °C	0 °C	−10 °C	−20 °C	−30 °C			
INR18650-35E	0.002	4.494	15.654	55.097	193.265	380.708			
INR18650-30Q	1.350	2.700	8.550	31.800	139.000	524.000			
ICR18650-26J	0.943	3.220	10.300	36.700	64.000	93.500			
INR 18650-25R	0.001	2.024	6.374	36.557	65.000	87.395			
ICR 18650-22P	0.028	5.380	27.300	90.800	262.131	1150.000			
INR18650-MJ1	1.550	5.880	15.800	43.600	205.661	230.310			
INR18650 M26	0.017	5.300	14.600	48.800	185.000	423.466			
NCR18650GA	10.000	40.700	96.834	22.835	110.000	145.000			
US18650 VTC5A	12.104	53.815	160.940	431.759	2.66E+04	5.17E+06			

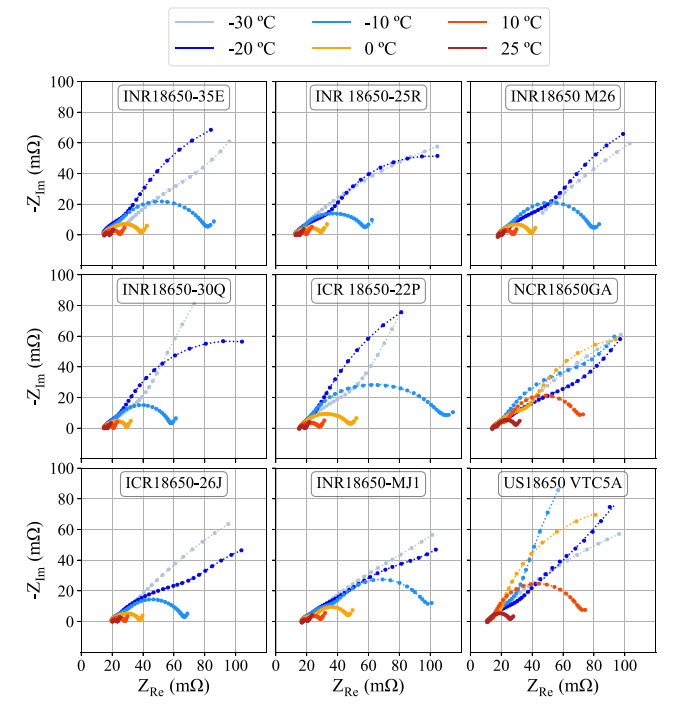


Fig. 6. Nyquist Plot representation of EIS Impedance measurements for all cells. Each color indicates a specific environmental temperature. Circular markers represent the measured EIS data while dotted lines indicate the fitted curves. (For interpretation of the references to color in this figure legend, the reader is referred to the web version of this article.)

INR18650-30Q demonstrated the highest relative capacity retention in the entire measured temperature range. The capacity of these cells has only decreased around 20% of their nominal capacity at $-30~^{\circ}\mathrm{C}$ with a discharge current of 1 A, whereas other cells could not be discharged. Another noteworthy cell is INR18650-35E, which, despite having worse capacity retention as the temperature decreases, is the one that can provide the highest energy values. However, some cells, such as INR18650-MJ1, NCR18650GA and US18650-VTC5A, delivered a low energy level during the discharge at $-30~^{\circ}\mathrm{C}$. This limitation significantly reduces their utility at such low temperatures.

In terms of initial voltage stability, due to the internal impedance of the cells, the voltage drops depending on the current demand from the battery. Therefore, cells with greater voltage stability are recommended for systems with sensitive power requirements, with the aim of enabling operation at higher currents over a wider temperature range. For example, microsatellites with an unregulated battery bus using a two-cell series configuration may have problems with the battery's minimum voltage limit. For that reason, cells with a low voltage drop are more suitable for this battery configuration. Thus, INR18650-30Q and INR18650-35E cells stand out among all the cells in this sense. On the contrary, NCR18650GA and US18650 VTC5A present a higher

initial voltage drop that can be difficult to manage by the Electrical Power System (EPS).

Concerning the thermal response during discharge tests, further differences have been found. Due to the Joule effect, cells with higher discharge currents exhibit increased temperature rise. As is studied in [36], around 54% of the total heat generation in a cylindrical Li-ion cell is due to this effect. For that reason, cells with higher internal resistance will have a greater temperature increase. Nevertheless, cells with excessive heat generation could not be appropriate for their longevity [42]. This heat generation is due to electrical losses in the cell, which can be critical in microsatellites with compromised energy due to a reduced available volume for their EPS. Based on this, INR18650-25R and INR18650-30Q, which have moderate thermal behavior, would be a better option for a high efficiency energy storage system.

4.2. EIS analysis

EIS results provide additional insight into impedance behavior across temperatures and frequencies, indicating which cells can sustain lower impedance at cold temperatures. Analyzing Fig. 7, the cells INR18650-25R and INR18650-30Q provide lower real impedance with low temperatures at a glance, as well as lower capacitive behavior. By contrast, NCR18650GA and US18650 VTC5A presents the poorest performances at low temperatures.

Concerning the equivalent circuit model analysis, the main parameter affected by lower temperatures is R_2 . Research has shown [43, 44], that charging at reduced temperatures accelerates degradation more than the discharge process does under similarly low-temperature conditions. Therefore, the cells with the largest R_2 values in cold environments are less appropriate for use in applications where low temperatures are prevalent.

In the context of space applications, foolproof in an EPS is essential due to the high costs and time required to launch a microsatellite. The space environment exposes electronic components to levels of radiation not encountered inside the Earth's protective atmosphere [45]. Such environment can cause issues like Single Event Effects (SEE) and Total Ionizing Dose (TID) [46]. An SEE occurs when high-energy particles penetrate the PN junction of integrated circuits, potentially leading to sudden faults. On the other hand, TID refers to the cumulative energy deposited by radiation particles passing through a semiconductor material, which can degrade circuit performance over time. For deep space missions, if a redundant system is intended, every effort must be made to prevent or minimize potential system failures caused by these radiation events. For instance, if the thermal control circuit had a failure, the battery might be subjected to charging at low temperatures, a situation that could compromise its longevity and performance [43,47]. For that reason, the cells INR18650-25R, INR18650-30Q and ICR18650-26J, which are the cells with the lowest R₂ values at lower temperatures, are likely to be the most suitable candidates for these conditions and have a greater resilience to cold temperature-induced degradation during charging.

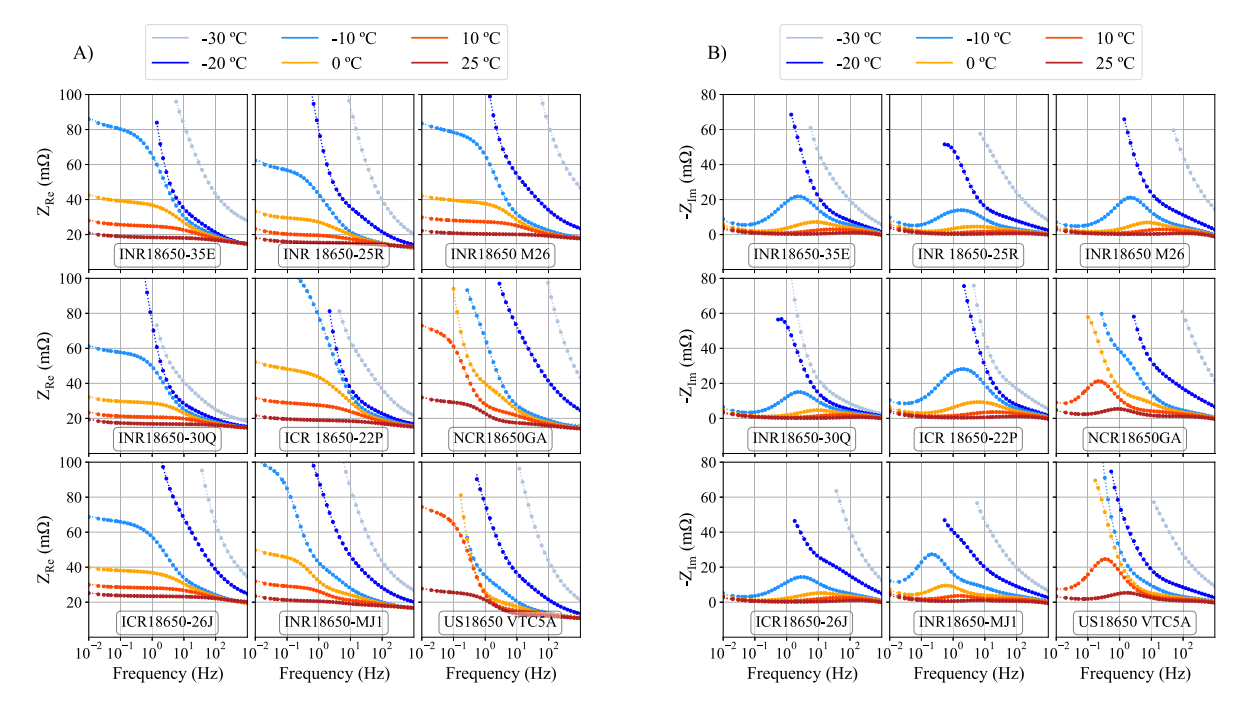


Fig. 7. EIS Impedance measurement (A) Real part of the impedance plot as a function of frequency; (B) Imaginary part of the impedance plot as a function of frequency. Each color indicates a specific environmental temperature. (For interpretation of the references to color in this figure legend, the reader is referred to the web version of this article.)

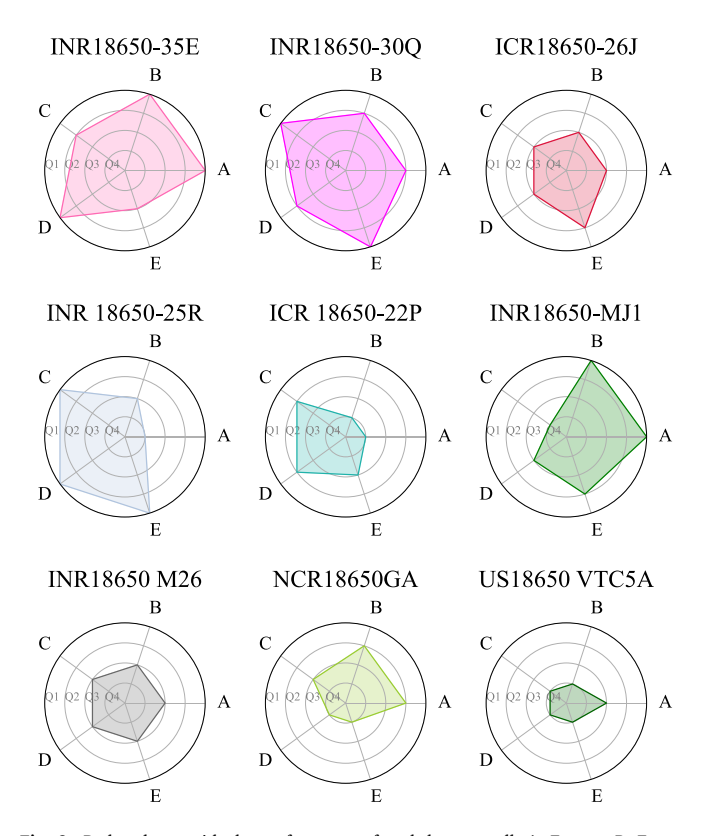


Fig. 8. Radar charts with the performance of each battery cell. A: Energy, B: Energy density, C: Capacity retention, D: Voltage drop, E: Impedance rising.

However, it is worth noting that certain deep space missions may experience temperatures above 0 °C during the charging process, particularly during full illumination periods, as has been shown in Fig. 1. Under these conditions, the $\rm R_2$ parameter becomes less critical, as higher ambient temperatures mitigate the adverse effects associated

with charging at low temperatures. Nevertheless, considering the $\rm R_2$ parameter remains valuable, as it ensures flexibility and resilience across a range of operating environments, supporting robust cell selection for varied mission profiles.

4.3. Additional comments and future work

The results of this study highlight several areas for future research. In addition to the conducted discharge and impedance tests of this work, further evaluations are crucial to determine the optimal cell choice for microsatellite applications. As has been commented before, one important assessment is Total Ionizing Dose (TID) testing, typically conducted with a Co-60 gamma radiation source [48], to evaluate the cell's resilience in the radiation environment of space. According to the literature [16], several commercially available 18650 cells of this study have been tested for radiation tolerance. After the study presented in this paper, eight cells of the INR18650-30Q model of this study were subjected to TID testing up to 100 krads with the Co-60 irradiator of the 'Centro Nacional de Aceleradores (CNA)' in Seville, Spain. The cells under tests demonstrate a correct resistance to radiation exposure with an average degradation of 2.00%.

5. Conclusion

The findings of this study provide a comprehensive evaluation of COTS 18650 Li-ion cells, focusing on their performance under temperature conditions relevant to deep space missions. The results underscore the critical importance of selecting appropriate cells during battery design. Proper cell selection can significantly improve efficiency, ensure reliable power delivery, and expand operational temperature ranges.

To provide a comprehensive comparison of each cell's performance across key parameters, Fig. 8 presents a radar chart for each cell, evaluating energy capacity, energy density, low-temperature capacity retention, voltage drop stability, and temperature rise. The evaluation is based on quartiles, allowing a clear assessment of where each cell stands in relation to the others for each characteristic. In these radar charts, the highest values are associated with the first quartile (Q1), while the lowest values correspond to the fourth quartile (Q4).

Considering these results, the INR18650-30Q is the most promising candidate for microsatellite deep space missions. This cell provides balanced performance across all critical factors, ensuring stable power, minimal energy loss, and adequate thermal behavior under a low temperature environment.

However, it is also necessary to highlight the performance of other cells which also stand out from the remaining cells. The INR18650-25R shows less voltage drop and less impedance rise than most other cells, although its energy density is much lower than the rest. This makes it a practical choice for space missions where the battery is only used in short eclipse periods, knowing that there are better options in terms of energy density. The INR18650-35E also deserves to be mentioned, as it is the highest capacity cell that performs well at low temperatures. However, its impedance increment at low temperatures may accelerate their degradation, so it should be interesting to analyze this its long-term durability before using them. Another option to be considered is the INR18650-MJ1 cell. While it is true that their behavior at low temperatures is not the best, it is the cell with the higher values of energy and energy density. These characteristics could enable the allocation of more energy to a thermal management system, ensuring the battery remains within a safe temperature range during operation. The operation at low temperatures of the remaining cells do not spotlight over the above-named.

Moreover, although this study focuses on the discharge performance and EIS analysis of the selected Li-ion cells under various temperature conditions, it is significant to highlight the importance of the life characteristics of the cells and their resistance to radiation. For that reason, future work should focus on further characterizing these cells under additional environmental stressors, such as radiation exposure, extended storage periods and cycle life, to validate their long-term suitability for deep space missions.

CRediT authorship contribution statement

P. Casado: Writing – original draft, Visualization, Software, Investigation, Formal analysis, Data curation. J.M. Blanes: Writing – review & editing, Supervision, Project administration, Funding acquisition, Conceptualization. A. Garrigós: Writing – review & editing, Supervision, Project administration, Funding acquisition, Conceptualization. D. Marroquí: Writing – review & editing, Methodology, Investigation, Conceptualization. C. Torres: Writing – review & editing, Software, Investigation, Data curation.

Declaration of competing interest

The authors declare that they have no known competing financial interests or personal relationships that could have appeared to influence the work reported in this paper.

Acknowledgments

This work was supported by the European Union NextGenerationEU and Generalitat Valenciana under Grant ASFAE/2022/21. Authors thank the Seville 'Centro Nacional de Aceleradores' (CNA) for allowing us to use their installations for the TID tests.

Appendix A. Supplementary data

Supplementary material related to this article can be found online at https://doi.org/10.1016/j.jpowsour.2025.236552.

Data availability

Data will be made available on request.

References

- V. Zancan, A. Paravano, G. Locatelli, P. Trucco, Evolving governance in the space sector: From Legacy Space to New Space models, Acta Astronaut. 225 (2024) 515–523.
- [2] A. Golkar, 23 overview of the new space CubeSat market, Next Gener. CubeSats SmallSats. (2023) 605–620.
- [3] Y. Tang, W. Ip, K. Yung, Z. Bi, Industrial information integration in deep space exploration and exploitation: Architecture and technology, J. Ind. Inf. Integr. 42 (2024) 100721.
- [4] J. Carrasco, F. García, H. Alavés, J. Palazón, Review of design strategies and benefits for electronic assemblies operating at low temperatures in space applications, J. Space Explor. (2018).
- [5] X. Lin, K. Khosravinia, X. Hu, J. Li, W. Lu, Lithium plating mechanism, detection, and mitigation in lithium-ion batteries, Prog. Energy Combust. Sci. 87 (2021) 100953
- [6] I. Lalinde, A. Berrueta, J. Arza, P. Sanchis, A. Ursúa, On the characterization of lithium-ion batteries under overtemperature and overcharge conditions: Identification of abuse areas and experimental validation, Appl. Energy 354 (2024) 122205
- [7] T. Barrera, Spacecraft Lithium-Ion Battery Power Systems, John Wiley, 2023.
- [8] AEA AEA Technology powers mission to Mars, Aircr. Eng. Aerosp. Technol. 75 (2003) aeat.2003.12775faf.009.
- [9] F. Krause, J. Loveland, M. Smart, E. Brandon, R. Bugga, Implementation of commercial Li-ion cells on the MarCO deep space CubeSats, J. Power Sources. 449 (2020) 227544.
- [10] J. Estaller, A. Kersten, M. Kuder, T. Thiringer, R. Eckerle, T. Weyh, Overview of battery impedance modeling including detailed state-of-the-art cylindrical 18650 lithium-ion battery cell comparisons, Energies. 15 (2022) 3822.
- [11] N. Zatta, B. Cesaro, E. Cin, G. Carraro, G. Cristofoli, A. Trovò, A. Lazzaretto, M. Guarnieri, Holistic testing and characterization of commercial 18650 lithium-ion cells, Batter. 10 (2024) 248.
- [12] S. Baksa, W. Yourey, Consumer-based evaluation of commercially available protected 18650 cells, Batter. 4 (2018) 45.
- [13] J. Bae, Electrical modeling and impedance spectra of lithium-ion batteries and supercapacitors, Batter. 9 (2023) 160.
- [14] V. Muenzel, A. Hollenkamp, A. Bhatt, J. Hoog, M. Brazil, D. Thomas, I. Mareels, A comparative testing study of commercial 18650-format lithium-ion battery cells, J. Electrochem. Soc. 162 (2015) A1592–A1600.
- [15] F. Krause, J. Ruiz, S. Jones, E. Brandon, E. Darcy, C. Iannello, R. Bugga, Performance of commercial li-ion cells for future NASA missions and aerospace applications, J. Electrochem. Soc. 168 (2021) 040504.
- [16] NASA State-of-the-Art of Small Spacecraft Technology 2023 Edition, NASA, 2024.
- [17] J. Zaragoza-Asensio, S. Pindado, J. Pérez-Álvarez, Li-ion battery for space missions based on COTS cells: Mechanical analysis and design, Egypt. J. Remote. Sens. Space Sci. 24 (2021) 311–317.
- [18] L. Wildfeuer, M. Lienkamp, Quantifiability of inherent cell-to-cell variations of commercial lithium-ion batteries, eTransportation 9 (2021) 100129.
- [19] She-Wu, P. Lee, Storage fading of a commercial 18650 cell comprised with NMC/LMO cathode and graphite anode, J. Power Sources 349 (2017) 27–36.
- [20] P. Lee, She-Wu, W. Pang, V. Peterson, The storage degradation of an 18650 commercial cell studied using neutron powder diffraction, J. Power Sources 374 (2018) 31–39.
- [21] P. Keil, A. Jossen, Charging protocols for lithium-ion batteries and their impact on cycle life—An experimental study with different 18650 high-power cells, J. Energy Storage 6 (2016) 125–141.
- [22] Y. Li, M. Bai, Z. Zhou, W. Wu, C. Hu, L. Gao, X. Liu, Y. Li, Y. Song, Thermal management for the 18650 lithium-ion battery pack by immersion cooling with fluorinated liquid, J. Energy Storage 73 (2023) 109166.
- [23] U. Koleti, C. Zhang, R. Malik, T. Dinh, J. Marco, The development of optimal charging strategies for lithium-ion batteries to prevent the onset of lithium plating at low ambient temperatures, J. Energy Storage 24 (2019) 100798.
- [24] X. Wang, X. Wei, Q. Chen, J. Zhu, H. Dai, Lithium-ion battery temperature online estimation based on fast impedance calculation, J. Energy Storage 26 (2019) 100052
- [25] S. Liu, J. Chen, C. Zhang, L. Jin, Q. Yang, Experimental study on lithium-ion cell characteristics at different discharge rates, J. Energy Storage 45 (2022) 103418.
- [26] P. Vyroubal, T. Kazda, Equivalent circuit model parameters extraction for lithium ion batteries using electrochemical impedance spectroscopy, J. Energy Storage 15 (2018) 23–31.
- [27] N. Meddings, M. Heinrich, F. Overney, J. Lee, V. Ruiz, E. Napolitano, S. Seitz, G. Hinds, R. Raccichini, M. Gaberšček, J. Park, Application of electrochemical impedance spectroscopy to commercial li-ion cells: A review, J. Power Sources 480 (2020) 228742.
- [28] J. Guo, Y. Xu, P. Li, K. Pedersen, M. Gaberšček, D. Stroe, Can electrochemical impedance spectroscopy be replaced by direct current techniques in battery diagnosis? ChemPhysChem. 25 (2024).
- [29] S. Cui, S. Lyu, Y. Ma, K. Wang, Improved informer PV power short-term prediction model based on weather typing and AHA-VMD-MPE, Energy 307 (2024) 132766.

- [30] Y. Shang, S. Wang, N. Tang, Y. Fu, K. Wang, Research progress in fault detection of battery systems: A review, J. Energy Storage 98 (2024) 113079.
- [31] H. Nunes, J. Martinho, J. Fermeiro, J. Pombo, S. Mariano, M. Rosário Calado, Impedance analysis and parameter estimation of lithium-ion batteries using the EIS technique, IEEE Trans. Ind. Appl. 60 (2024) 5048–5060.
- [32] F. Santoni, A. Angelis, A. Moschitta, P. Carbone, M. Galeotti, L. Cinà, C. Giammanco, A. Carlo, A guide to equivalent circuit fitting for impedance analysis and battery state estimation, J. Energy Storage. 82 (2024) 110389.
- [33] M. Singh, J. Kaiser, H. Hahn, Thick electrodes for high energy lithium ion batteries, J. Electrochem. Soc. 162 (2015) A1196–A1201.
- [34] W. Xie, Z. Zhang, X. Gao, Understanding the limitations of thick electrodes on the rate capability of high-energy density lithium-ion batteries, Electroch. Acta. 493 (2024) 144396.
- [35] P. Patel, G. Zhang, G. Nelson, Assessing the impact of electrode structure on the fast charge performance of lithium-ion batteries, J. Electrochem. Soc. 170 (2023) 010501
- [36] X. Zhang, Thermal analysis of a cylindrical lithium-ion battery, Electroch. Acta. 56 (2011) 1246–1255.
- [37] A. Abdollahi, X. Han, G. Avvari, N. Raghunathan, B. Balasingam, K. Pattipati, Y. Bar-Shalom, Optimal battery charging. Part I: Minimizing time-to-charge, energy loss, and temperature rise for OCV-resistance battery model, J. Power Sources 303 (2016) 388–398.
- [38] J. Yang, C. Du, W. Liu, T. Wang, L. Yan, Y. Gao, X. Cheng, P. Zuo, Y. Ma, G. Yin, J. Xie, State-of-health estimation for satellite batteries based on the actual operating parameters health indicator extraction from the discharge curves and state estimation, J. Energy Storage 31 (2020) 101490.
- [39] D. Zhang, C. Tan, T. Ou, S. Zhang, L. Li, X. Ji, Constructing advanced electrode materials for low-temperature lithium-ion batteries: A review, Energy Rep. 8 (2022) 4525–4534.

- [40] H. Liu, Z. Wei, W. He, J. Zhao, Thermal issues about Li-ion batteries and recent progress in battery thermal management systems: A review, Energy Convers. Manag. 150 (2017) 304–330.
- [41] S. Zhang, K. Xu, T. Jow, The low temperature performance of Li-ion batteries, J. Power Sources 115 (2003) 137–140.
- [42] K. Maher, A. Boumaiza, R. Amin, Understanding the heat generation mechanisms and the interplay between joule heat and entropy effects as a function of state of charge in lithium-ion batteries, J. Power Sources 623 (2024) 235504.
- [43] S. Zhang, K. Xu, T. Jow, Electrochemical impedance study on the low temperature of Li-ion batteries, Electroch. Acta 49 (2004) 1057–1061.
- [44] M. Petzl, M. Kasper, M. Danzer, Lithium plating in a commercial lithium-ion battery – a low-temperature aging study, J. Power Sources 275 (2015) 799–807.
- [45] L. Chang, W. Lin, Y. Chou, J. Lin, C. Lung, I. Chen, K. Hou, G. Gacal, Y. Chiu, Y. Wang, H. Chou, C. Chao, J. Liu, T. Hsiao, I. Cho, T. Date, M. Urata, M. Taeda, K. Tanaka, N. Vasovic, N. Keegan, The deep space radiation probe: Development of a first lunar science payload for space environment studies and capacity building, Adv. Space Res. (2024).
- [46] Q. Huang, J. Jiang, An overview of radiation effects on electronic devices under severe accident conditions in NPPs, rad-hardened design techniques and simulation tools, Prog. Nucl. Energy 114 (2019) 105–120.
- [47] M. Petzl, M. Danzer, Nondestructive detection, characterization, and quantification of lithium plating in commercial lithium-ion batteries, J. Power Sources 254 (2014) 80–87.
- [48] Y. Kimoto, H. Koshiishi, H. Matsumoto, T. Goka, Total dose orbital data by dosimeter onboard tsubasa (MDS-1) satellite, IEEE Trans. Nucl. Sci. 50 (2003) 2301–2306.